SUPPLEMENTARY MATERIAL

MRI-based computational modeling of blood flow and nanomedicine deposition in patients with peripheral arterial disease

Shaolie S. Hossain[1,*], Yongjie Zhang[2], Xiaoyi Fu[2], Gerd Brunner[3,4], Jaykrishna Singh[1], Thomas J. R. Hughes[5], Dipan Shah[3], Paolo Decuzzi[1,*]

[1]Department of Translational Imaging and Department of Nanomedicine, Houston Methodist Research Institute, Houston, TX
[2]Department of Mechanical Engineering, Carnegie Mellon University, Pittsburgh, PA
[3]Methodist DeBakey Heart & Vascular Center, Houston Methodist Research Institute, Houston, TX
[4]Division of Atherosclerosis and Vascular Medicine, Department of Medicine, Baylor College of Medicine, Houston, TX
[5]Institute for Computational Engineering and Sciences, The University of Texas at Austin, Austin, TX

[*]Currently at Department of Molecular Cardiology, Texas Heart Institute, Houston, TX

Supplementary Figure 1 Blood flow features at peak velocity during systole at **A)** baseline and **B)** 24-months post-intervention. Streamlines depicting flow direction (arrows) are presented along with velocity magnitude contours at cross-sections taken at a (I) proximal, a (II) distal and an (III) intermediate ("mean") location near the constriction.

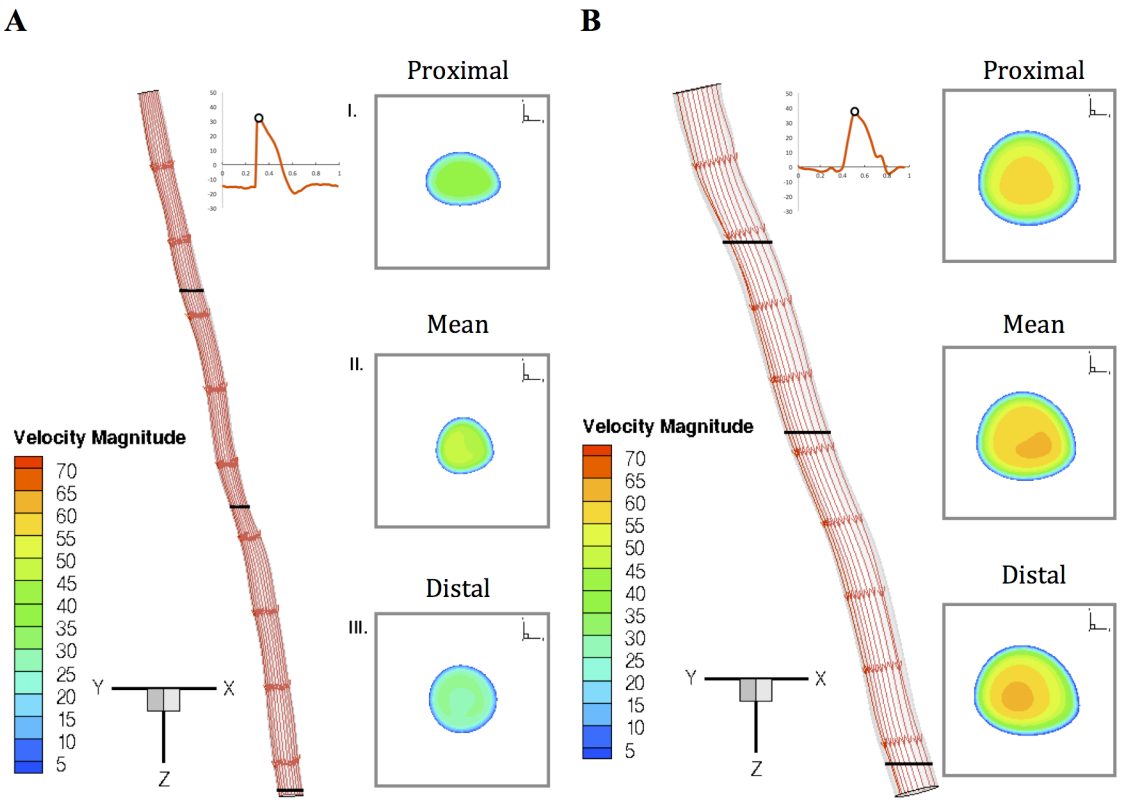

Supplementary Figure 2A: The blood velocity profiles represent right limb at baseline for a I) proximal (solid) and a II) distal (dashed) location. Velocities are obtained from phase contrast (PC) sequences with cardiac cycle duration of 1 s and represent mean values averaged over the luminal cross-section of the superficial femoral artery (SFA).

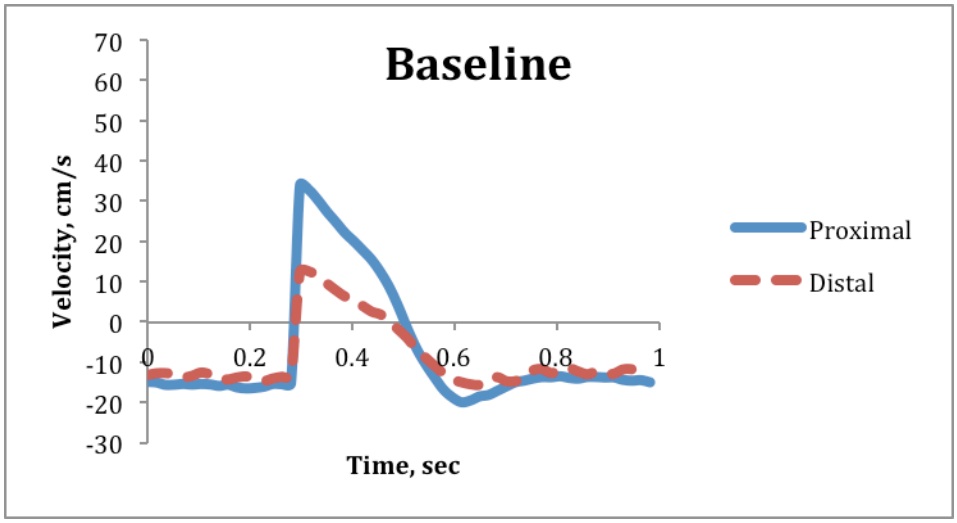

Supplementary Figure 2B Blood flow rate measured over a cardiac cycle at baseline (solid) and 24-months post-intervention (dots), resulting in an approximately 500% increase in peak flow rate.

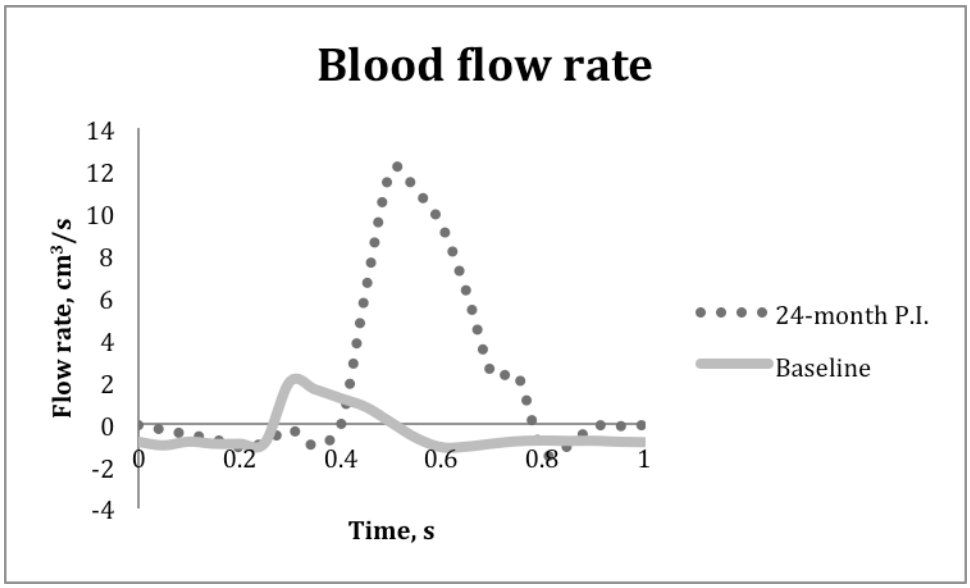

Supplementary Figure 2C: The blood velocity profiles represent right limb at 24-months post-intervention (P.I.) for a I) proximal (solid) and a II) distal (dashed) location. Velocities are obtained from PC sequences with cardiac cycle duration of 1 s and represent mean values averaged over the luminal cross-section of the SFA.

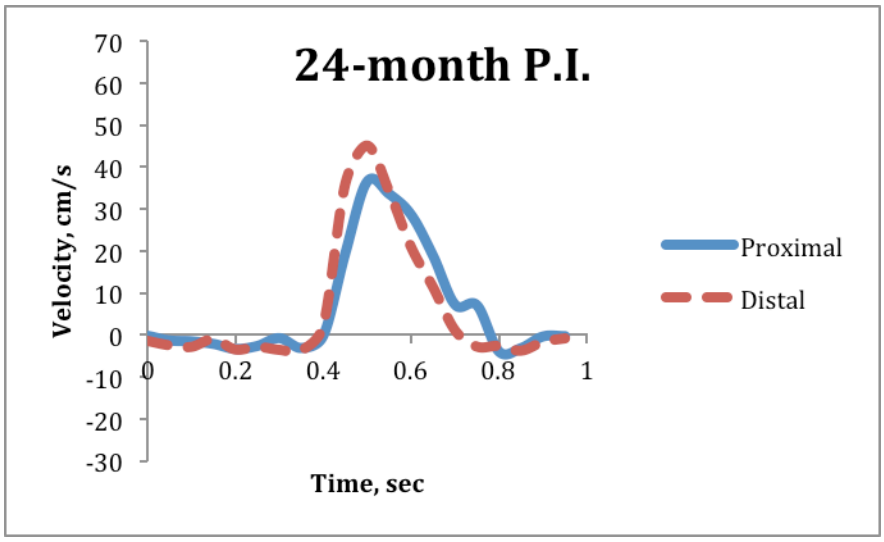

Table S1: Statistical quantities associated with TAWSS and OSI distributions

	Case	Mean	Skewness	Kurtosis
WSS	Baseline	2.7364	1.2744	4.8735
	24 Mo PI	2.1265	0.2319	2.1409
OSI	Baseline	0.2982	0.1009	2.8409
	24 Mo PI	0.2261	0.6150	2.6449

Supplementary Figure 3 Two different contours, (a) OSI and (b) WSS concentration (normalized), are merged (c) for both baseline (top) and 24-months post-intervention configurations. Here the unrolled geometries are presented. Bright yellow regions in (c) indicate low WSS along with higher OSI values.

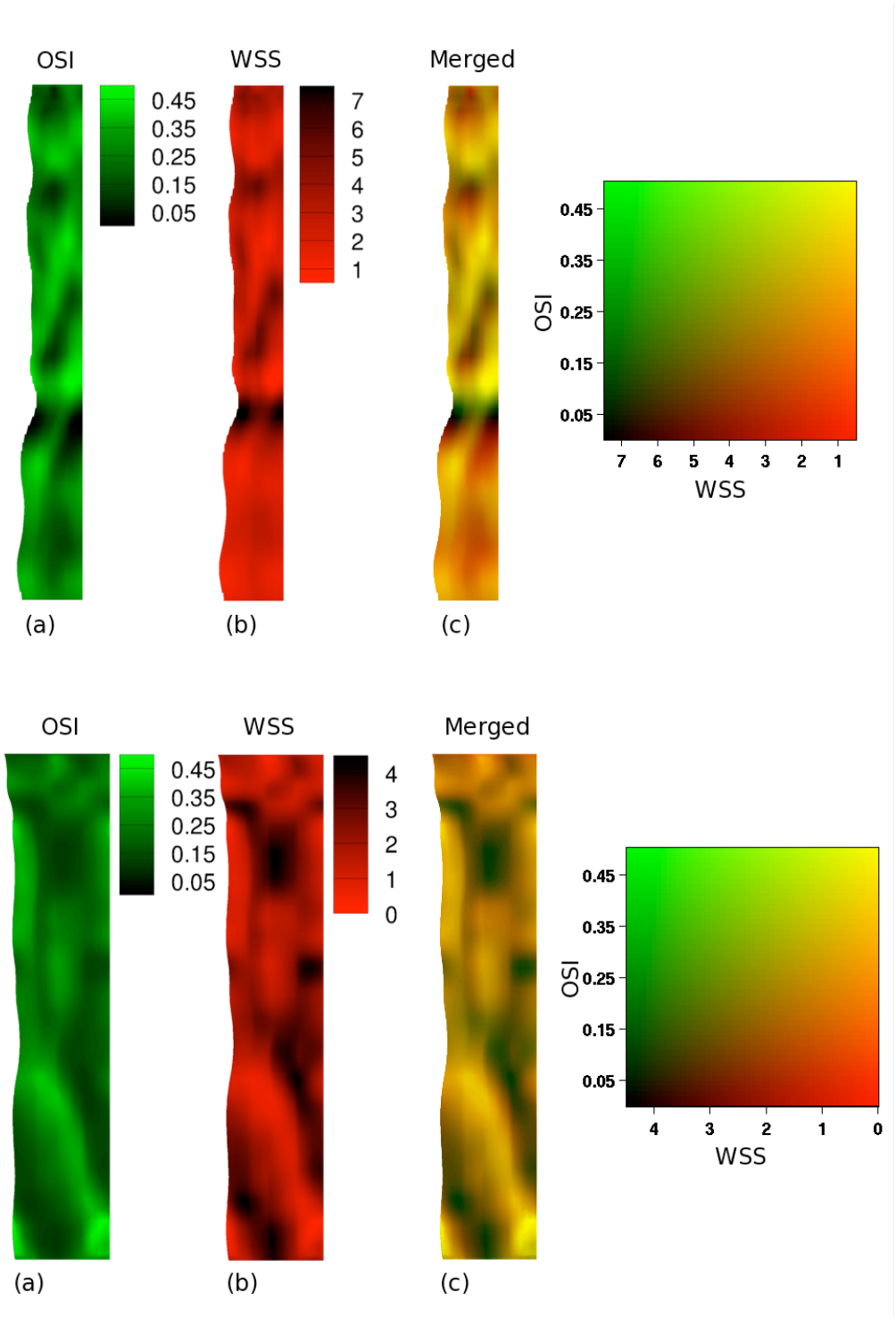

Supplementary Figure 4: Time evolution of particle (d_p = 100 nm) volumetric concentration (in blood) at baseline normalized by its concentration at the inlet C^0.

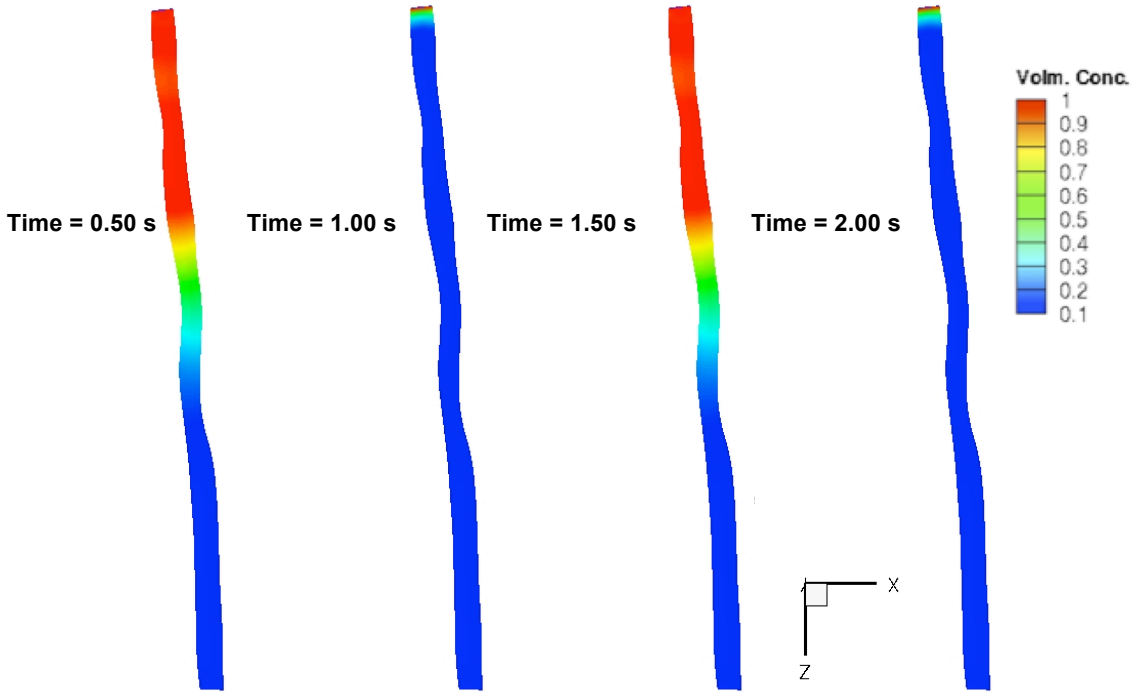

Supplementary Figure 5: Time evolution of particle (d_p = 100 nm) volumetric concentration (in blood) at 24-months post-intervention normalized by its concentration at inlet C^0.

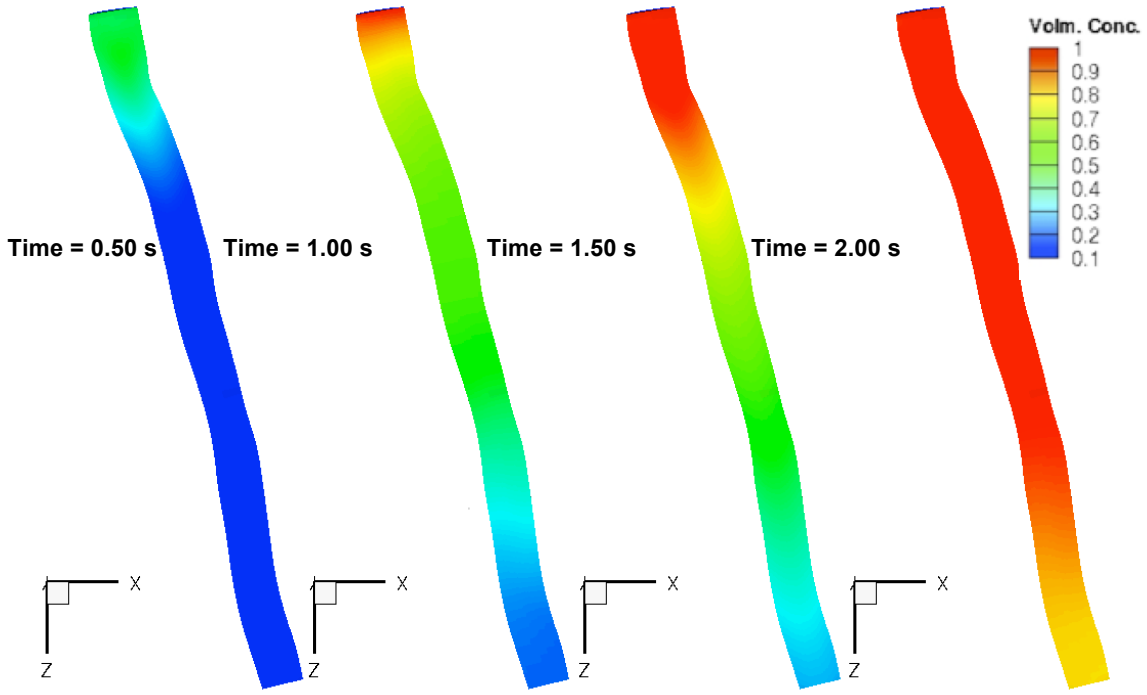

Supplementary Figure 6: Spatial distribution of VCAM-1 expression at **A)** baseline and **B)** 24-months post-intervention. The quantities are reported as a factor of unstimulated VCAM-1 expression under static conditions (mr/mr_0)

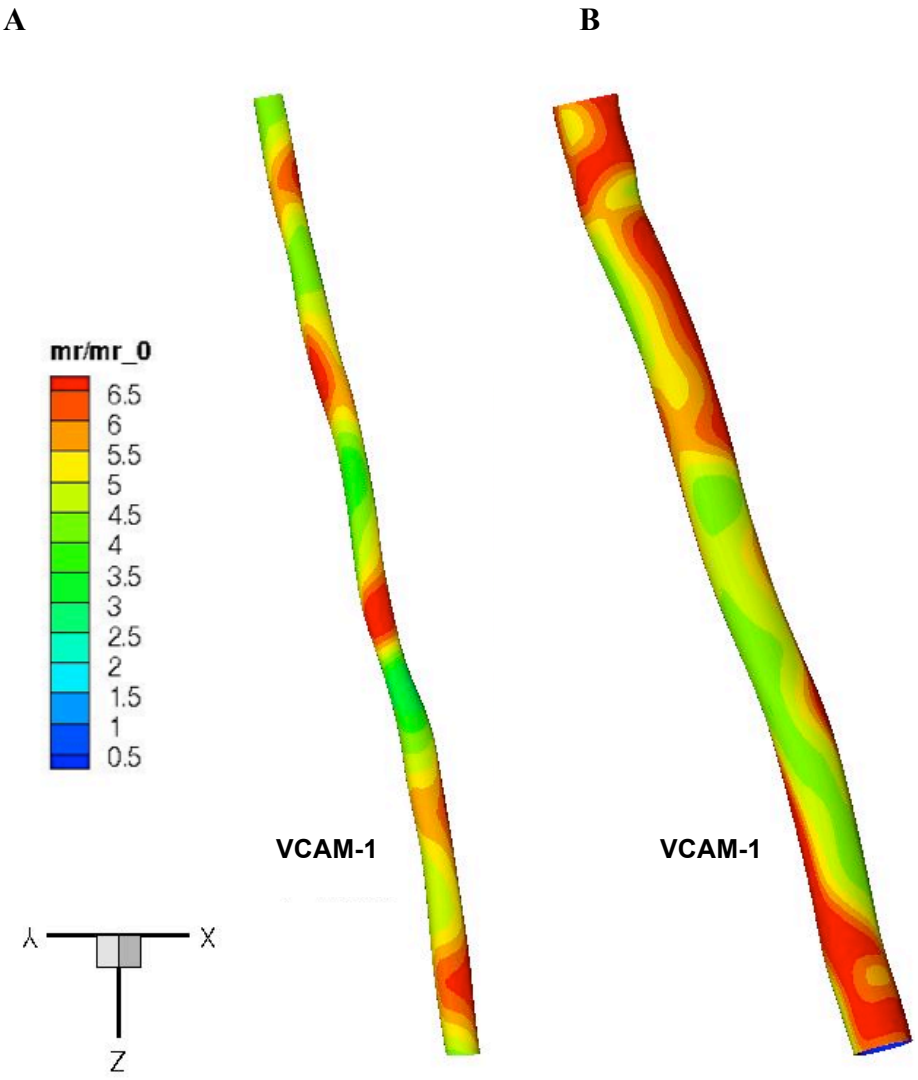

Supplementary Figure 7: Spatial distribution pattern for particles at baseline when receptor density is a function of local wall shear stress. Side by side comparison of **A)** ICAM-1, **B)** VCAM-1 and **C)** E-selectin directed particles in terms of their surface density (#/cm^2) at t = 10 s. Here particles were released in silico for 10 cardiac cycles from an NP bolus placed at the inlet.

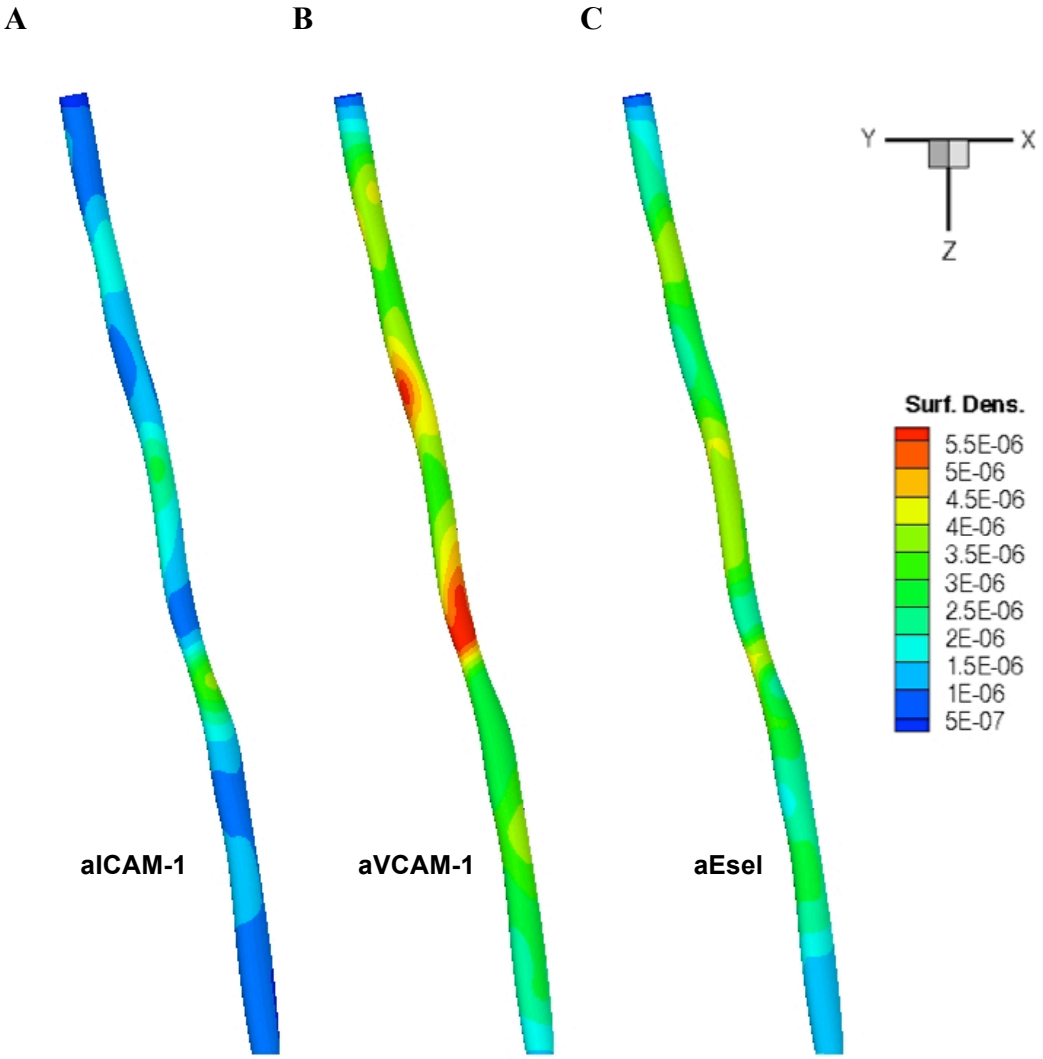

Supplementary Figure 8: Spatial distribution pattern for targeted particles at 24-months post-intervention when receptor density is a function of local shear stress. Side by side comparison of ICAM-1, VCAM-1 and E-selectin directed particles in terms of their surface density (#/cm^2) at t = 10 s. Here particles were released in silico for 10 cardiac cycles from an NP bolus placed at the inlet.

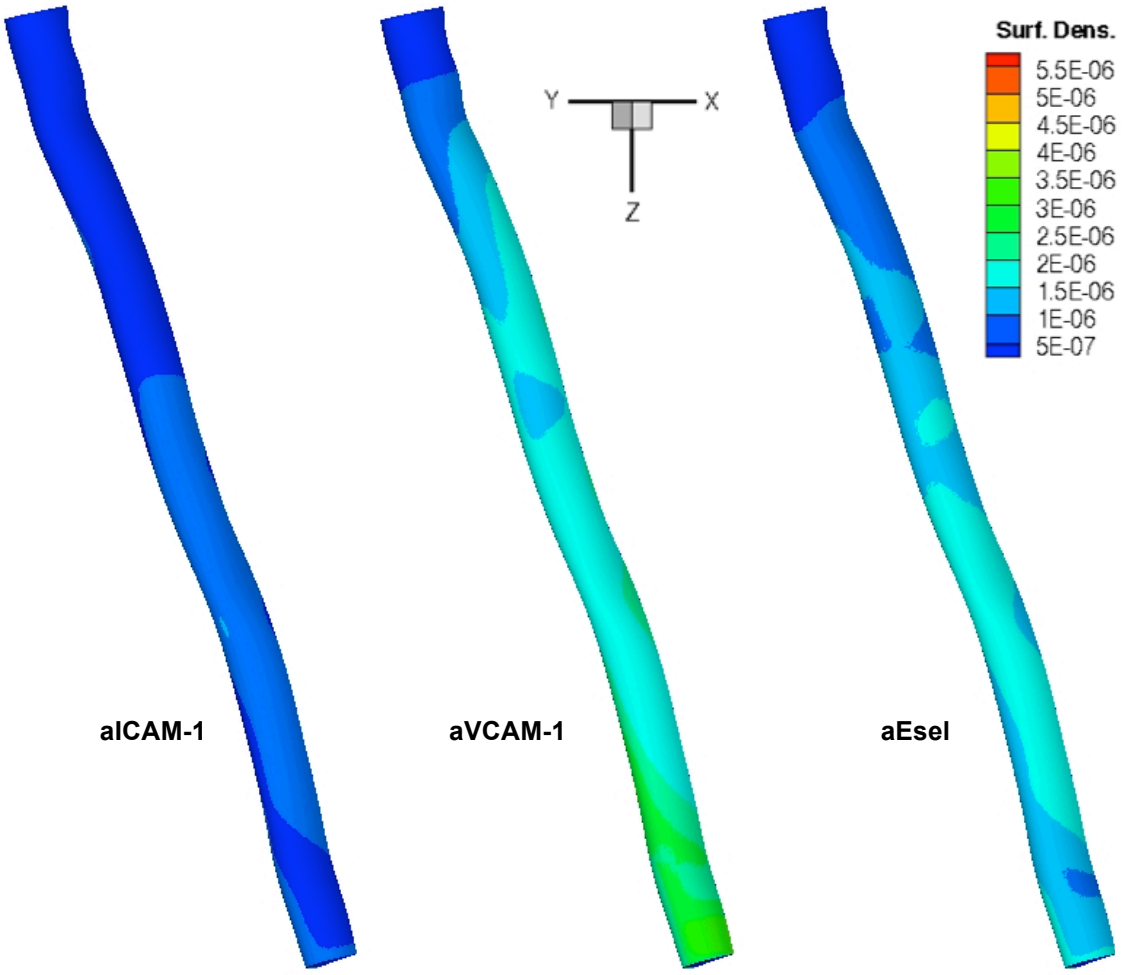

Supplementary Figure 9 aVCAM-1, aICAM-1 and aEsel NP distribution at Baseline (dark grey) and 24-months post-intervention (24M PI). Each bar of the histograms represents the amount of normalized area with a defined range of NP surface density (1e-6 NPs/cm^2). Here, the x-axis labels denote the upper bound of each range of NP density. For example, 1 represents a surface density of 10^{-6} NPs per square centimeters.

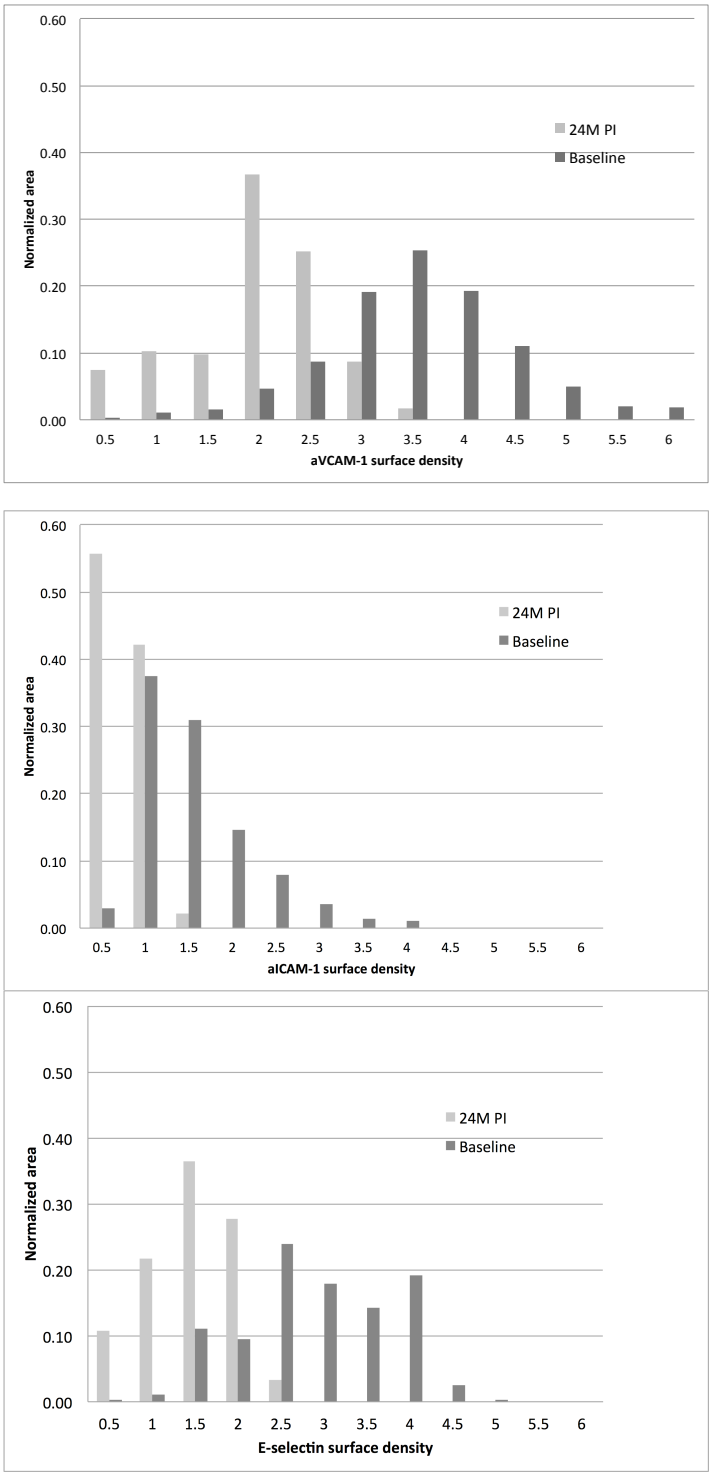

Supplementary Figure 10 Two different contours, (a) WSS and (b) aVCAM-1 concentration (normalized), are merged (c) for both baseline (top) and 24-months post-intervention configurations. Here the unrolled geometries are presented. Bright yellow regions in (c) indicate low WSS along with higher concentrations of aVCAM-1.

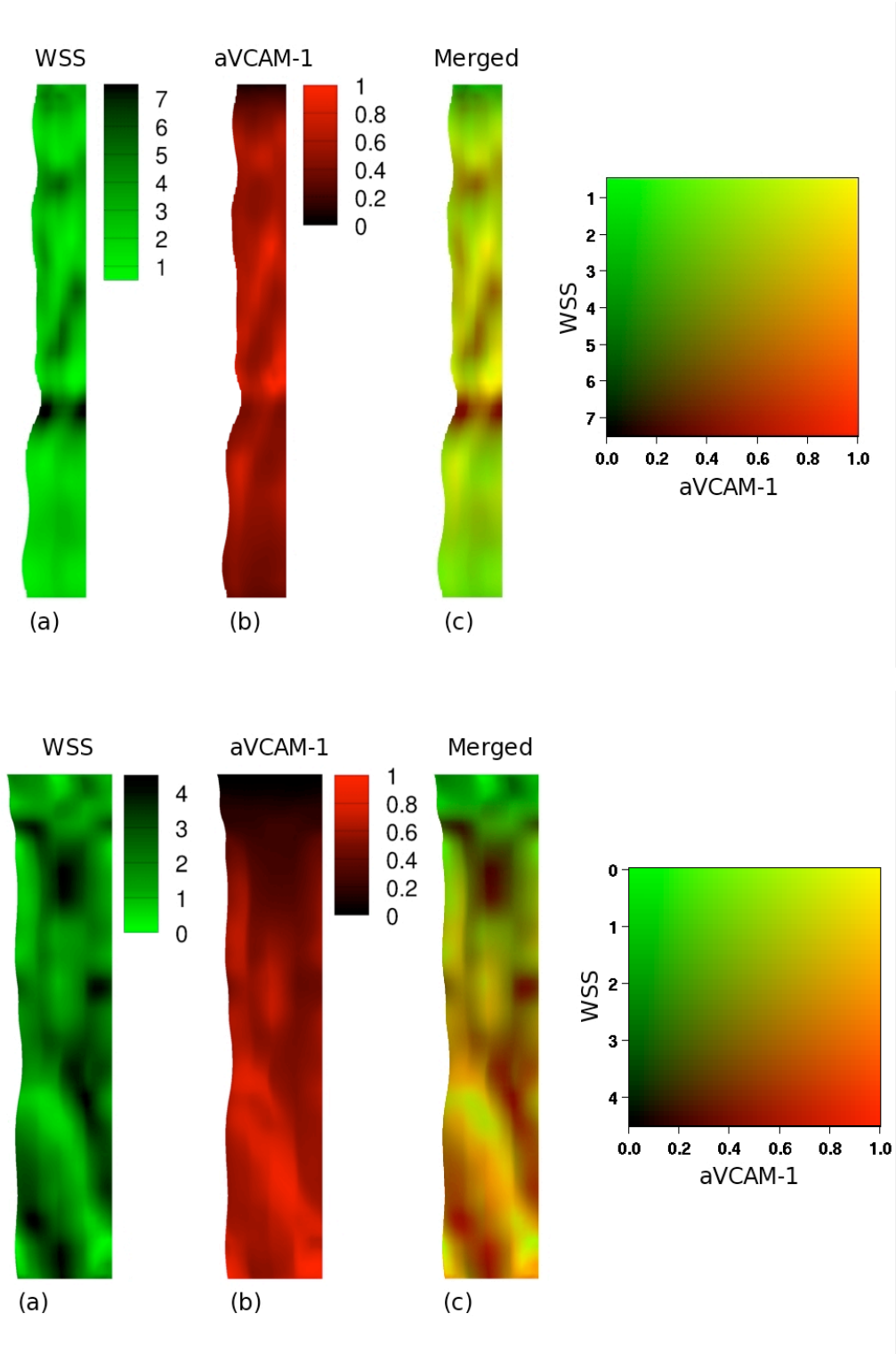

Supplementary Figure 11 Two different contours, (a) RRT and (b) aVCAM-1 concentration (normalized), are merged (c) for both baseline (top) and 24-months post-intervention cases. Here the unrolled geometries are presented. Bright yellow regions in (c) indicate high RRT along with higher concentrations of aVCAM-1. Note RRT values 5 and above were ignored.